A transcriptional constraint mechanism limits the homeostatic response to activity deprivation in mammalian neocortex

Abbreviated Title: HLF and TEF regulate homeostatic plasticity

Vera Valakh, Xiaoyue Aelita Zhu, Derek Wise, Stephen Van Hooser, Robin Schectman, Isabel Cepeda, Ryan Kirk, Sean O'Toole, Sacha B. Nelson.

Proofs and correspondence to:

Sacha B Nelson, MD, PhD, Brandeis University

Department of Biology, MS 008, 415 South Street, Waltham, MA 02454,

Email: nelson@brandeis.edu

Declaration of Interest: The authors declare no competing financial interests.
Acknowledgements: This research was supported by the National Institute of Neurological Disease and Stroke and by the Simons Foundation for Autism Research.

Abstract

Healthy neuronal networks rely on homeostatic plasticity to maintain stable firing rates despite changing synaptic drive. These mechanisms, however, can themselves be destabilizing if activated inappropriately or excessively. For example, prolonged activity deprivation can lead to rebound hyperactivity and seizures. While many forms of homeostasis have been described, whether and how the magnitude of homeostatic plasticity is constrained remains unknown. Here we uncover negative regulation of cortical network homeostasis by PAR bZIP family of transcription factors. In their absence the network response to prolonged activity withdrawal is too strong and this is driven by exaggerated upregulation of recurrent excitatory synaptic transmission. These data indicate that transcriptional activation is not only required for many forms of homeostatic plasticity but is also involved in restraint of the response to activity deprivation.

Introduction

Neuronal networks are equipped with a set of homeostatic plasticity mechanisms that enable them to rebalance activity following perturbations during development, learning, or disease. Homeostatic plasticity can alter the intrinsic excitability of individual neurons, as well as the strength and number of both excitatory and inhibitory synapses (Davis, 2006; Turrigiano and Nelson, 2004). Synaptic changes can occur post- (Turrigiano et al., 1998) or presynaptically (Delvendahl and Müller, 2019) and may scale quantal amplitudes and alter the frequency of quantal events. These changes are homeostatic because they occur in the direction needed to rebalance the network after activity perturbation. Especially during development, homeostatic mechanisms are strong and can be maladaptive if they overshoot or are activated inappropriately (Nelson and Valakh, 2015).

Despite recognition of the significance of homeostatic plasticity, whether and how its strength is normally constrained has remained unknown. Downregulation of the strength of homeostatic plasticity could potentially provide protection against inappropriate or excessive activation of these mechanisms. However, such negative regulators of homeostatic plasticity have not been previously described.

Here we investigate the role of the proline and acidic amino acid-rich basic leucine zipper (PAR bZIP) family of transcription factors (TF) in homeostatic plasticity. The family consists of hepatic leukemia Factor (HLF), thyrotroph embryonic factor (TEF), and albumin D-site-binding protein (DBP) which are thought to act as transcriptional activators, as well as E4 Promoter-Binding Protein 4 (E4BP4, currently known as Nfil3) that acts as a transcriptional repressor (Mitsui et al., 2001). All 4 family members share the same DNA binding motif. DBP is a circadian gene controlled by CLOCK and oscillates with circadian rhythm (Ripperger et al., 2000). Other family members are also controlled by CLOCK (Li et al., 2017). However, while these TFs typically have oscillatory behavior in peripheral tissue, they do not oscillate in the brain outside of the SCN (Gachon et al., 2004). Loss of HLF, TEF and DBP has been associated with epilepsy (Gachon et al., 2004; Hawkins and Kearney, 2016; Rambousek et al., 2020) suggesting they are important in regulating network activity.

In order to investigate the role that gene transcription plays in regulating the neuronal response to activity deprivation, we profiled changes in gene expression engaged during homeostatic plasticity and found that prolonged activity deprivation activates a robust transcriptional program

involving the PAR bZIP TF family members HLF and TEF. Both act to restrain the expression of homeostatic plasticity. While they have limited effects on network function at baseline, they strongly suppress the upregulation of homeostatic changes, mainly by regulating recurrent excitatory synaptic connections. Together these results indicate that homeostatic plasticity is itself subject to activity-dependent regulation and is transcriptionally restrained by the PAR bZIP TFs HLF and TEF.

Results

PAR bZIP transcripts increase during activity deprivation

Certain forms of homeostatic plasticity require transcription (Goold and Nicoll, 2010; Ibata et al., 2008) and activity perturbation results in changes in gene expression (Schaukowitch et al., 2017). We hypothesized that among the differentially expressed genes, some induce or regulate homeostatic changes. To identify novel genes involved in the homeostatic response to activity deprivation, we measured gene expression in excitatory and inhibitory neurons in organotypic slice cultures following a global decrease in activity. We cut coronal slices including neocortex at p7 and cultured them for 5 days. During this culture period the neurons reform connections, and spontaneous bouts of activity, termed up states, emerge (Johnson and Buonomano, 2007; Koch et al., 2010). To broadly block activity, we applied the voltage-gated sodium channel blocker tetrodotoxin, TTX (0.5μM), for 5 days during an early developmental period (equivalent postnatal day, EP, 12-17). This manipulation induces a robust homeostatic program and profoundly changes network dynamics (Koch et al., 2010; Schaukowitch et al., 2017). To characterize the changes in gene expression, we sorted deep layer (L5 and L6) pyramidal and PV^+ interneurons and performed RNA sequencing to look for transcripts that change following prolonged silencing. Inactivity activates a robust transcriptional program of both positively and negatively affected genes (Figure 1A) consistent with data from dissociated hippocampal cultures (Schaukowitch et al., 2017). To identify potential regulators of homeostatic plasticity, we looked for genes upregulated in the TTX condition. We identified a PAR bZIP family of transcription factors including *Hlf*, *Tef*, and *Dbp*. Expression levels of *Dbp* are much lower than those of *Hlf* and *Tef* (<3 TPM in excitatory and PV+ inhibitory neurons), suggesting that this last family member may play a more limited role in the neocortex. Both *Hlf* and *Tef* are robustly upregulated after 5 days of activity deprivation in both excitatory (Fold Change TTX/control; FC = 2.6, 2.5; adjusted p-value; p_{adj} = 1.3e-8, 3.8e-4,) and inhibitory neurons (FC = 7.0, 2.1; p_{adj} = 4.6e-39, 2.0e-3), while *Nfil3* and *Dbp* were not (FC = 0.51, 1.9; p_{adj}= 0.49, 0.80, excitatory; FC= 1.2, 1.4; p_{adj}= 0.84, 0.79 inhibitory).

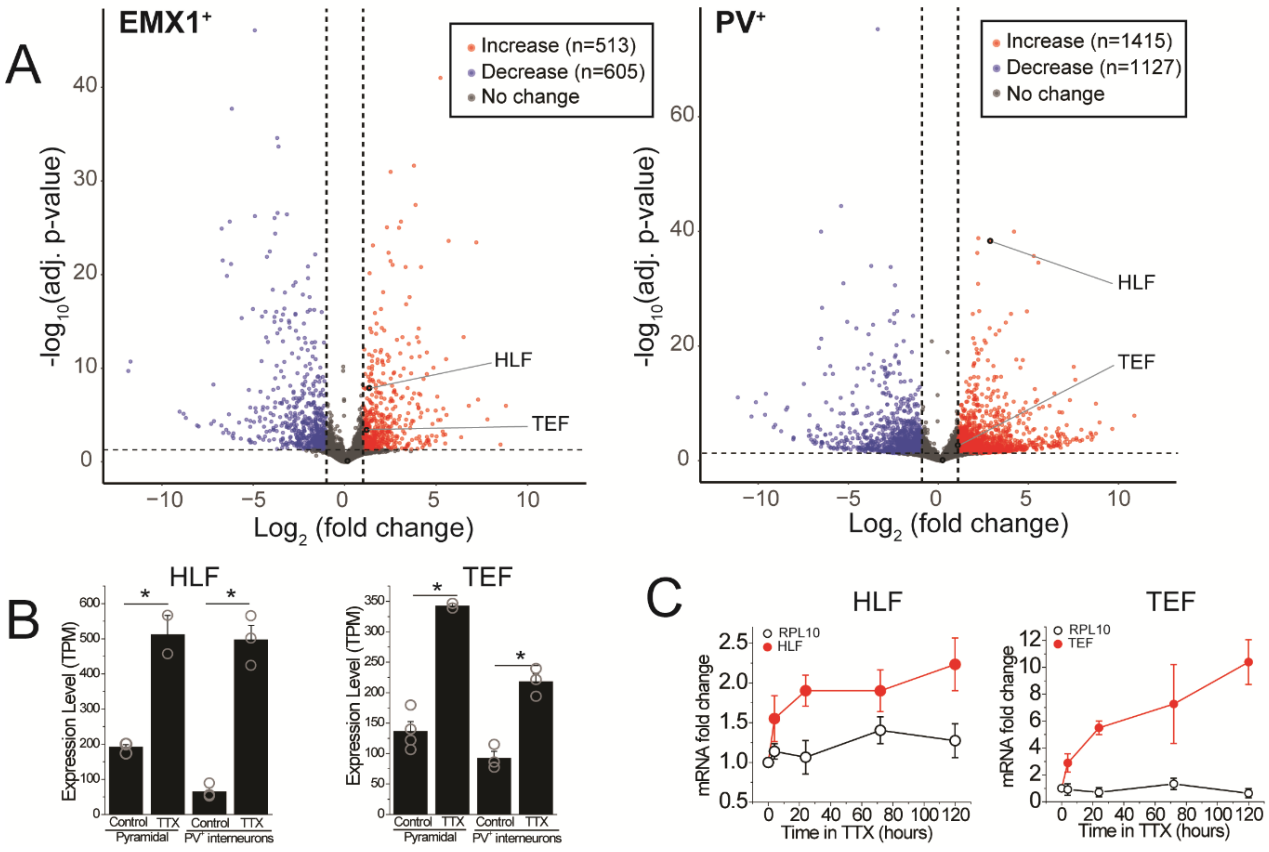

Figure 1. RNA-sequencing identifies transcripts affected by activity deprivation including the PAR bZIP family of transcription factors. (A) Volcano plots of bulk RNA-seq from sorted fluorescently labeled pyramidal cells (left) and PV+ interneurons (right). Dashed lines indicate a Fold-change of 2 and adjusted p-value of 0.05. Differential expression analysis revealed that TTX resulted in upregulation (513 in pyramidal, 1415 in PV$^+$ interneurons) as well as downregulation (605 in pyramidal, 1127 in PV$^+$ interneurons) of genes, among which *Hlf* and *Tef* were identified as upregulated with activity block in both excitatory and inhibitory neurons. Statistical analysis (Wald test followed by Benjamini-Hochberg correction) reveals that *Hlf* and *Tef* are significantly upregulated in both pyramidal cells and PV$^+$ interneurons, while *Dbp* and *Nfil3* are not significantly altered in either cell type. **(B)** Bar graphs displaying transcript per million (TPM) values of *Hlf* (left panel) and *Tef* (right panel) in pyramidal cells (left) and interneurons (right) in control and 5-day TTX treated slices. Bars are mean values, open symbols are individual experiments. **(C)**. Quantitative real-time PCR analysis of *Hlf* and *Tef* expression in whole cortex lysates following a time course of activity deprivation. Two-way ANOVA reveals significant differences between *Hlf*/*Tef* and RPL10 ($p<0.05$) and between *Hlf*/*Tef* expression at different time points ($p<0.05$).

To validate this finding and to further dissect the time course of PAR bZIP transcription factors expression, we isolated the whole cortex from slice cultures and measured *Hlf* and *Tef* transcript levels at various time points during activity deprivation using real-time quantitative PCR. We find that upregulation occurs soon after activity withdrawal, since by 4 hours of TTX application the level of both TFs is already significantly elevated (Figure 1C), consistent with previous findings in dissociated hippocampal cultures (Schaukowitch et al., 2017). We also find that *Hlf* and *Tef* continue to increase with time, suggesting that their upregulation correlates with how long the network has been silenced.

PAR bZIP TFs restrain network homeostatic plasticity

Since *Hlf* and *Tef* are progressively upregulated during prolonged TTX treatment, which can lead to subsequent epilepsy (Galvan et al., 2000; Scharfman, 2002), we entertained the hypothesis that they may contribute to the homeostatic increase in network excitability following activity deprivation. On the other hand, loss of function of members of the PAR bZIP family of TFs are also associated with epileptic phenotypes (Hawkins and Kearney, 2012, 2016; Rambousek et al., 2020). Specifically, triple knockout (TKO) *Hlf*$^{-/-}$/*Dbp*$^{-/-}$/*Tef*$^{-/-}$ mice have epilepsy (Gachon et al., 2004). One possibility that reconciles this apparent conflict is that instead of driving homeostatic changes, *Hlf* and *Tef* are upregulated in the TTX condition to restrain homeostatic responses. To test this hypothesis, we investigated the role that these TFs play in homeostatic plasticity. We induced homeostatic upregulation of network function by two-day TTX application in organotypic slice cultures and measured network activity after TTX removal.

As a read-out of network activity, we measured changes in intracellular calcium using virally-delivered GCaMP6f in primary somatosensory cortex (Figure 2A). In untreated slices at baseline, the neurons display population activity organized into complex, infrequent up states which are similar to those observed in vivo (Figure 2B, Sanchez-Vives and McCormick, 2000). The activity of cells from slices derived from the TKO are indistinguishable from wild type (WT) at baseline (Figure 2). After two days of TTX treatment, the frequency of the up states increases. To quantify network activity, we measured the frequency of Ca^{2+} peaks in each recording (see methods for detailed description of quantitative analysis). While 2 days of TTX incubation increases the peak frequency two-fold in WT slices, the same silencing duration produces a four-fold increase in the TKO slices (Figure 2). These data suggest that the PAR BZIP family of TFs normally functions to restrain homeostatic plasticity, and in their absence, the homeostatic response is exaggerated. Moreover, even though the mutation is associated with epilepsy, it does not make cortical neuronal circuits more excitable at baseline.

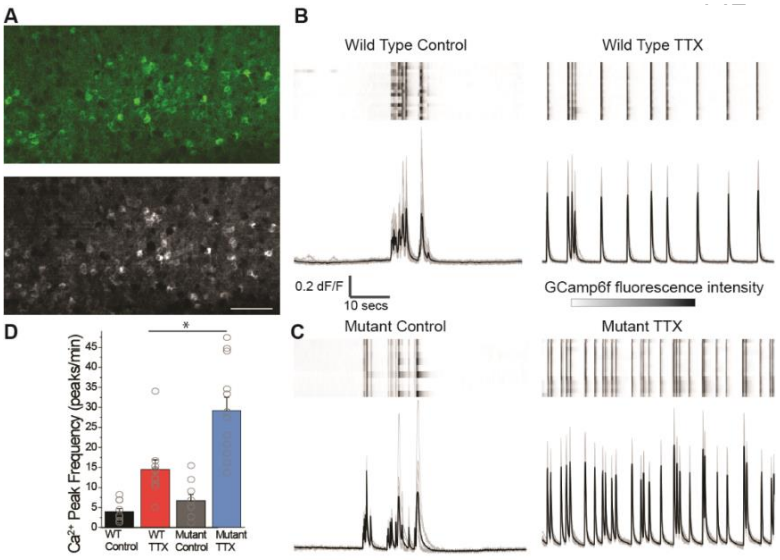

Figure 2. Calcium imaging reveals exaggerated response to activity deprivation in *Hlf*$^{-/-}$/*Dbp*$^{-/-}$/*Tef*$^{-/-}$ triple knockout (TKO) slices. (A). A confocal image of GCaMP6f fluorescence during an up state in wild type (WT) control slice (top panel) and a standard deviation projection of the same field of view of calcium signal during one minute of recording (bottom panel). Scale bar = 50µm. ROIs were manually selected around active cells identified by high standard deviation values. **(B,C)** GCaMP6f fluorescence heat map of selected ROIs (rows) during one minute of recording (top panels) also shown as overlapping traces (gray, bottom panels). and an average fluorescence (black trace, bottom panels) during one minute of recording in WT **(B)** and TKO (mutant) slices **(C)** from control (left) and TTX-treated conditions (right). **(D)** Quantification of peak frequency in GCaMP6f fluorescence traces. TTX treatment significantly increases peak frequency in WT slices. The increase is more dramatic in the TKO slices. Two-way ANOVA with Bonferroni correction for multiple comparisons to test statistical significance between conditions * p≤0.001.

Recovery from activity deprivation is unperturbed in the mutant slices

Homeostatic plasticity is thought to provide flexibility to the network and thus most forms are reversed after reintroduction of activity (Desai et al., 2002; Hobbiss et al., 2018; Koch et al., 2010; Wallace and Bear, 2004). Reversal involves a homeostatic reduction of abnormally elevated activity. Even when this involves symmetric opposing changes in the same biophysical parameters altered in the response to activity deprivation (such as with downscaling and upscaling of excitatory quantal amplitudes), the mechanisms involved typically differ (Stellwagen and Malenka, 2006; Sun and Turrigiano, 2011; Tan et al., 2015; Wang et al., 2017). To test whether the transcriptional restraint of homeostasis is required for such flexibility we asked whether the network is able to return back to baseline activity levels when the activity block is removed. We measured network activity right after silencing with TTX as well as following two days of incubation in the TTX-free media. In WT slices, activity deprivation causes hyperactivity evident from a two-fold rise in the peak frequency of the calcium activity. This exuberant activity is restored back to baseline levels within two days following restoration of action potential firing. In the mutant, even though the initial response to TTX is exaggerated, the network is also able to return to baseline levels following two days of recovery, indistinguishable from WT (Figure 2 Supplement 1). These data suggest that the recovery from a high activity state is not diminished in the mutant.

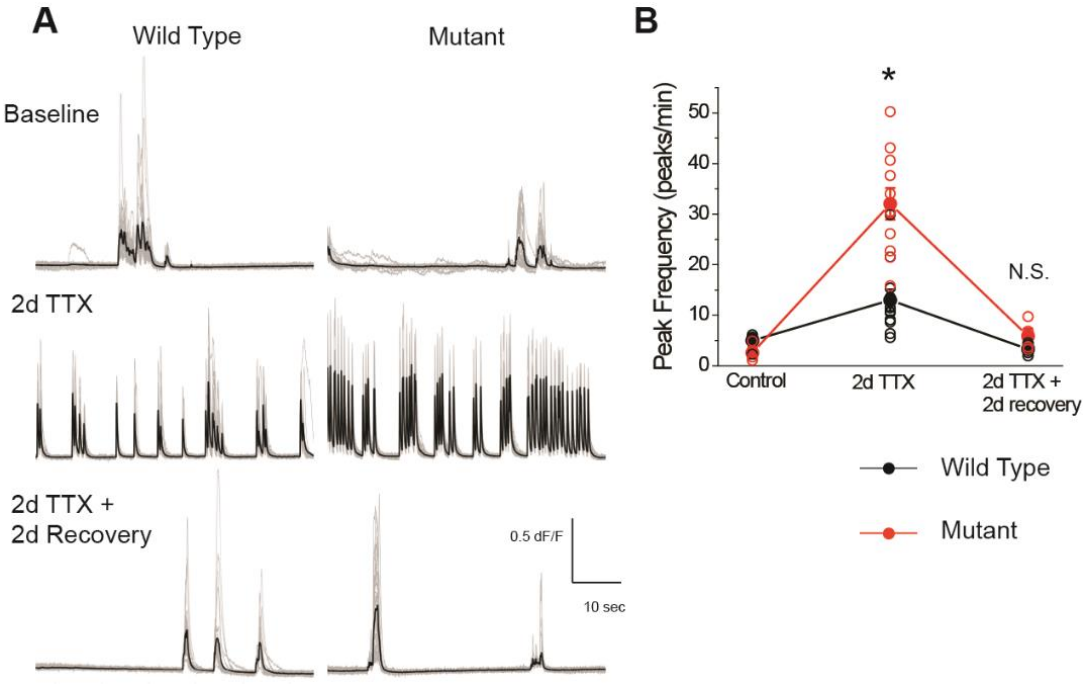

Figure 2, Supplemental 1. Ca^{2+} activity recovers to baseline levels following washout of TTX in both wild type and mutant slices. (A) Representative GCaMP6f fluorescence intensity over 1 minute of recording in WT (left panels) and TKO slices (right panels) during control (top row), immediately after TTX washout (middle row) and after two days of recovery following TTX washout (bottom row). **(B)** Quantification of peak frequency in each of the conditions in **(A)**. Open symbols are individual slice cultures, filled symbols are mean ± SEM. Although TTX incubation has a much stronger effect on spontaneous Ca2+ activity immediately after washout in mutant slices, the activity returns back to baseline in both genotypes. Two-way ANOVA followed by Bonferroni correction for multiple comparisons to test the difference between individual groups. * $p<0.05$, N.S. $p>0.05$.

Frequency, but not amplitude, of mEPSCs is disproportionately upregulated by deprivation in TKO slices

Network activity is unaltered in the mutant at baseline but the response to activity deprivation is exaggerated. To learn more about the mechanism by which *Hlf* and *Tef* restrain homeostatic plasticity, we probed the effects of TTX on excitatory synaptic transmission. Because of the high levels of spontaneous network activity, it was not feasible to study unitary action potential evoked transmission. Instead, to broadly assay the properties of excitatory synapses, we measured pharmacologically isolated miniature EPSCs in control and TTX-treated slices. We observed a robust upregulation of mEPSC amplitude following two days of activity deprivation, consistent with our understanding of homeostatic synaptic scaling (Turrigiano et al., 1998). We also observed a large increase in mEPSC frequency, which has also been described in this preparation (Koch et al., 2010) and in multiple other preparations (Wierenga et al., 2006). In the TKO mice, the synaptic scaling is unaffected (Figure 3 A,C) but the increase in mEPSC frequency in response to activity deprivation is more dramatic (Figure 3 B,D). Notably both the frequency and amplitude of mEPSCs are the same between WT and mutant slices at baseline which parallels our observations of network activity (Figure 2). These results suggest that the members of the PAR bZIP family of TFs function to restrain upregulation of mEPSC frequency in response to activity deprivation and this increase is correlated with changes in activity levels across the network.

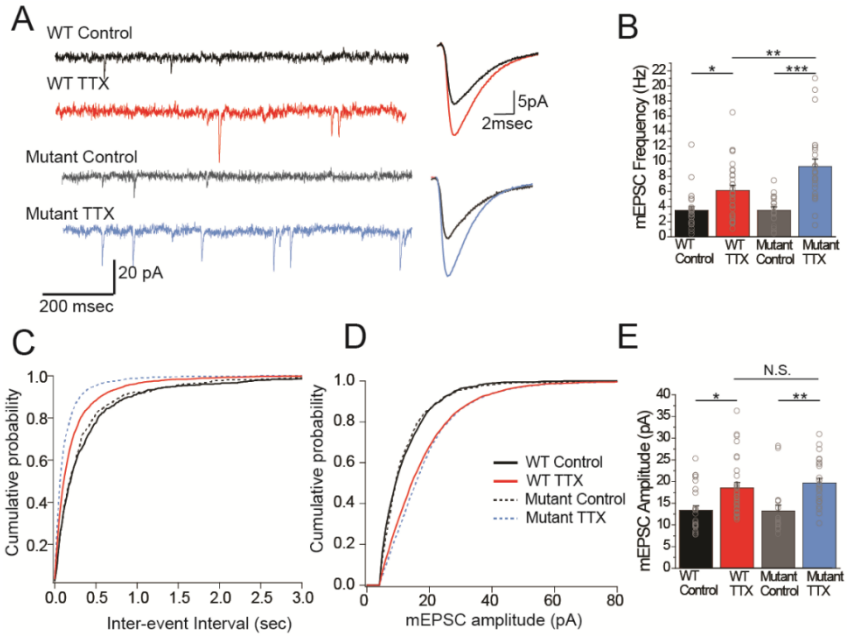

Figure 3. Frequency but not amplitude of excitatory synaptic currents is disproportionally upregulated in TTX-treated TKO slices. (A) Representative traces of mEPSC recordings from WT control (black), WT TTX-treated (red), TKO control (gray), and TKO TTX-treated (blue) slices. Right panel, average mEPSC waveforms for the same conditions. Both the frequency and the amplitude is increased in TTX-treated slices, however, the increase in frequency is more dramatic in TKO slices. **(B)** Quantification of mEPSC frequency for each condition. Colored bars with error bars are mean ± SEM, open circles are individual cells. **(C)** Cumulative probability histogram for mEPSC inter-event intervals in each condition. **(D)** Cumulative probability histogram for mEPSC amplitudes in each condition. (E) mEPSC amplitudes for each condition. *adj. $p < 0.05$, **adj. $p < 0.01$, ***adj. $p < 0.001$, N.S. – not significant, adj. $p > 0.05$, two-way ANOVA with Tukey post hoc test.

Neither the frequency nor amplitude of mIPSCs in pyramidal neurons in the TTX condition are affected in the TKO.

Since L5 pyramidal neurons also receive inhibitory input, which is also subject to homeostatic plasticity (Kilman et al., 2002; Kim and Alger, 2010), we wanted to determine whether the

response of mIPSCs to activity deprivation is also exaggerated in the mutant mice. In wild-type cultures, measurement of inhibitory input onto L5 pyramidal neurons revealed that both the amplitude and frequency of mIPSCs drop in response to activity deprivation (Figure 4). When we measured mIPSCs in pyramidal neurons from TKO slices, we saw a similar decrease in frequency following 48 hr TTX treatment, although the amplitude of the change was smaller than in the WT (Figure 4 B,C). In contrast, the mIPSC amplitude change is abolished: mIPSC amplitude is decreased at baseline compared to WT but did not show a further decrease after TTX treatment (Figure 4 D,E). However, the decreased amplitude in the untreated condition does not correlate with the unchanged baseline network activity levels (Figure 2), suggesting that the decrease of mIPSCs amplitude at baseline may be insufficient on its own to cause network hyperexcitability. Thus, both the amplitude and frequency of mIPSCs received by pyramidal neurons after activity deprivation are indistinguishable from the wild-type in the TKO slices, suggesting that homeostatic plasticity of mIPSCs is not driving the changes in the network activity following TTX treatment.

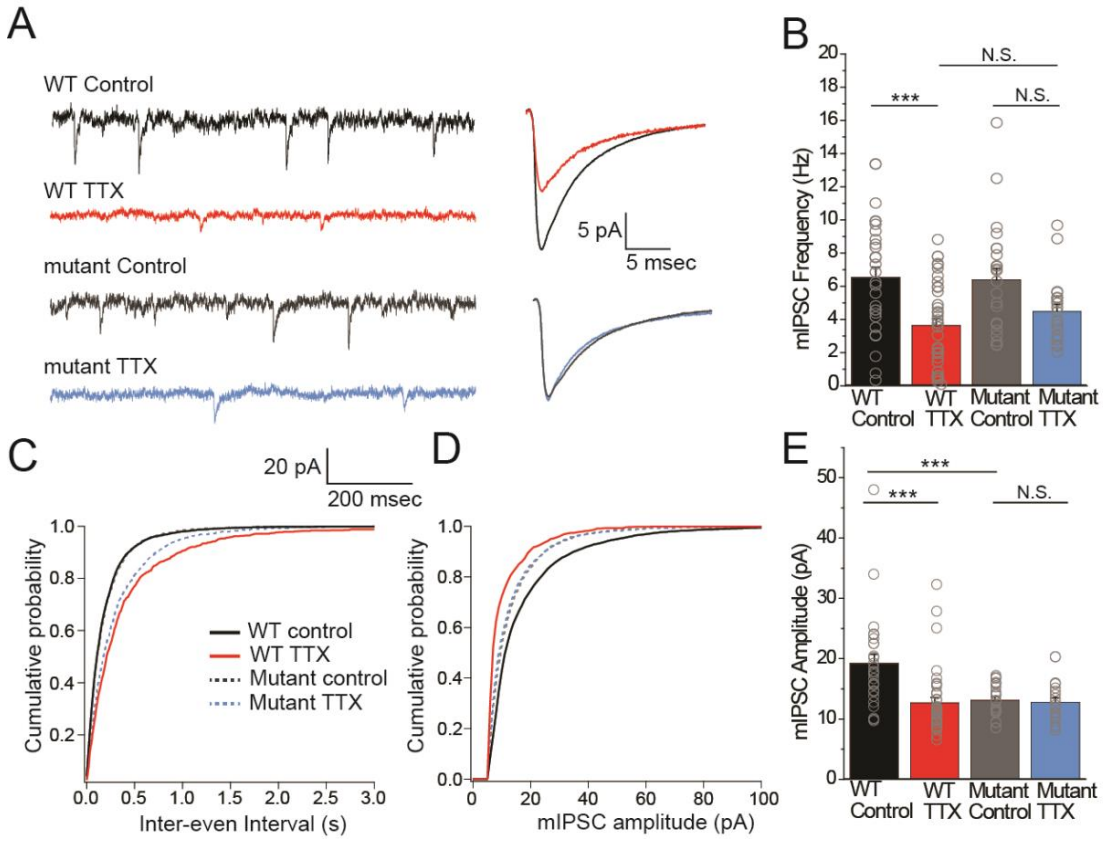

Figure 4. Inhibitory synaptic currents are not affected by the *Hlf*$^{-/-}$/*Dbp*$^{-/-}$/*Tef*$^{-/-}$ mutation in the TTX condition. (A) Representative traces of mIPSC recordings from WT control (black), WT TTX-treated (red), TKO control (gray), and TKO TTX-treated (blue) slices. Right panel, average mIPSC waveforms for the same conditions. TTX treatment results in a diminished effect on mIPSC frequency in TKO (adj. p = 0.14) and does not further decrease the amplitude of mIPSCs in TKO slices. **(B)** Quantification of mIPSC frequency. Colored bars with error bars are mean ± SEM, open circles are individual cells. In **B** and **E**, ***adj. p < 0.001, N.S. – not significant, adj. p >0.05 two-way ANOVA with Tukey post hoc test to compare between individual conditions. **(C)** Cumulative probability histogram for mIPSC inter-event intervals in each condition. **(D)** Cumulative probability histogram for mIPSC amplitudes in each condition. **(E)** Quantification of mIPSC amplitudes.

Intrinsic excitability of pyramidal neurons is unaffected in TKO slices.

Changes in neuronal excitability have also been described as part of the homeostatic response to activity deprivation (Desai et al., 1999; Karmarkar and Buonomano, 2006; Lambo and Turrigiano, 2013; Moore et al., 2018; Yoshimura and Rasband, 2014). We wanted to test whether changes in intrinsic excitability could be contributing to the exaggerated homeostatic response in the TKO slices similarly to mEPSCs. WT L5 pyramidal neurons become more excitable following prolonged activity deprivation (Figure 5; Desai et al., 1999). To account for difference in the proportion of adapting and non-adapting neurons (Hattox and Nelson, 2007) causing apparent changes in intrinsic excitability due to uneven sampling of the two groups, we measured the adaptation ratio of each cell and analyzed an equal number of adapting and non-adapting cells in each genotype. Changes in excitability due to activity deprivation are accompanied by a shift in the average adaptation ratio of the cells in both WT and TKO slices (control WT: 3.8±0.16, TTX WT: 0.72 ±0.22, TKO control: 0.46±0.25, TKO TTX: 0.71±0.33, two-way ANOVA significant difference between control and TTX and no significant difference between WT and TKO). Excitatory neurons in L5 in the slices prepared from TKO animals are equally excitable at baseline and also show upregulation of intrinsic excitability to the same extent (Figure 5). These results suggest that changes in intrinsic excitability are not driving the exaggerated network response to activity deprivation and this form of homeostatic plasticity is not under the control of the Par bZIP TF family.

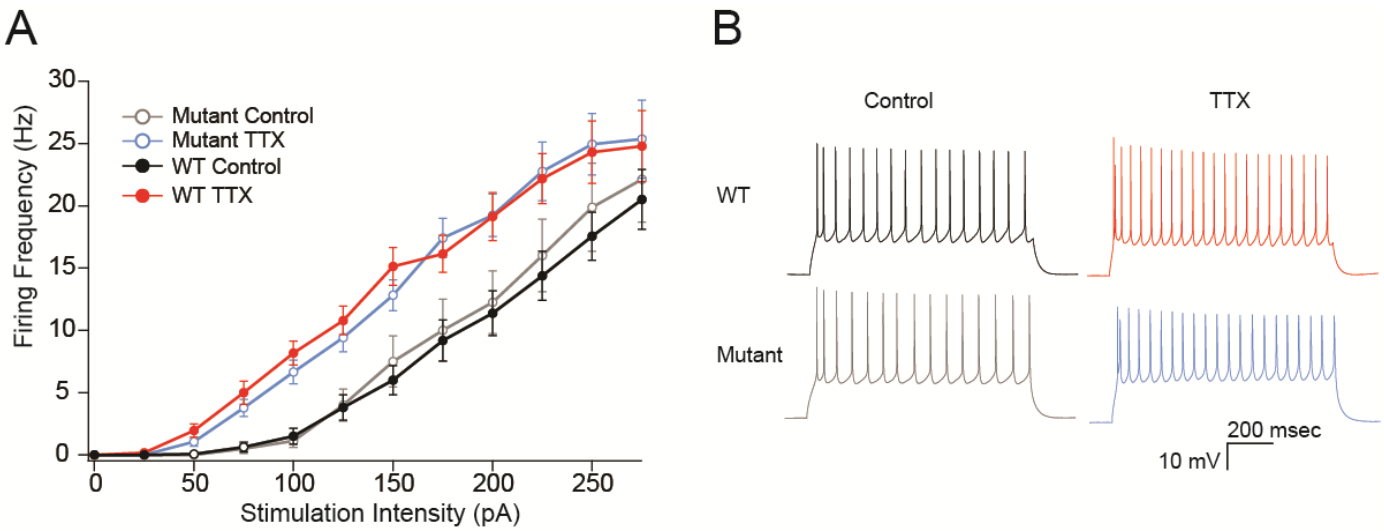

Figure 5. The effects of TTX on intrinsic excitability are not altered in TKO pyramidal neurons. (A) Comparisons of frequency-current relationships for layer 5 pyramidal neurons in control (black, closed circles) and TTX-treated (red, closed circles) WT slices, and in control (gray, open circles), and TTX-treated (blue, open circles) TKO slices. Two-day TTX treatment increases intrinsic excitability ($F(1,60) = 18$, $p < 0.001$) in both WT and TKO slice cultures to the same extent ($F(1,60) = 0.006$, $p = 0.94$, 3-way ANOVA). **(B)** Example traces of a train of action potentials from a pyramidal neuron in response to a 175pA 0.5s depolarizing current injection in control (left), TTX-treated (right), wild type (top), or TKO (bottom) slices.

PAR bZIP family members play unequal roles in restraining homeostatic plasticity

Expression of both *Hlf* and *Tef* increase in excitatory neurons following activity deprivation. Because all three Par bZIP family members form homo- and heterodimers and bind to the same PAR-response element (Gachon, 2007), they may be able to compensate for one another. To test whether both *Hlf*, *Tef*, and *Dbp* work together to regulate homeostatic plasticity or if they have unequal contributions to restraining network response to activity deprivation, we measured the homeostatic response while varying gene copy number of each transcription factor. None of the genotypes differed in their network activity at baseline (Figure 6, top panel). However, slices lacking both *Hlf* and *Tef* but that had either one or both copies of *Dbp* had an exaggerated response to 48hr of activity deprivation indistinguishable from the TKO mice (Figure 6). These data further demonstrate that *Dbp* is playing a limited role in the cortex and is unable to functionally compensate for the lack of the other two family members. On the other hand, deprived slices from mice lacking both copies of *Hlf* and *Dbp* and having just one intact copy of *Tef* had network activity within WT levels (Figure 6). Thus, a single copy of *Tef* was sufficient to maintain the normal degree of constraint of the homeostatic response. The response to TTX in animals lacking *Tef* and *Dbp* with only a single *Hlf* allele is intermediate (Figure 6). These data suggest that a single copy of *Tef* can functionally compensate for the lack of other family members in regulating homeostatic plasticity but even two copies of *Dbp* cannot.

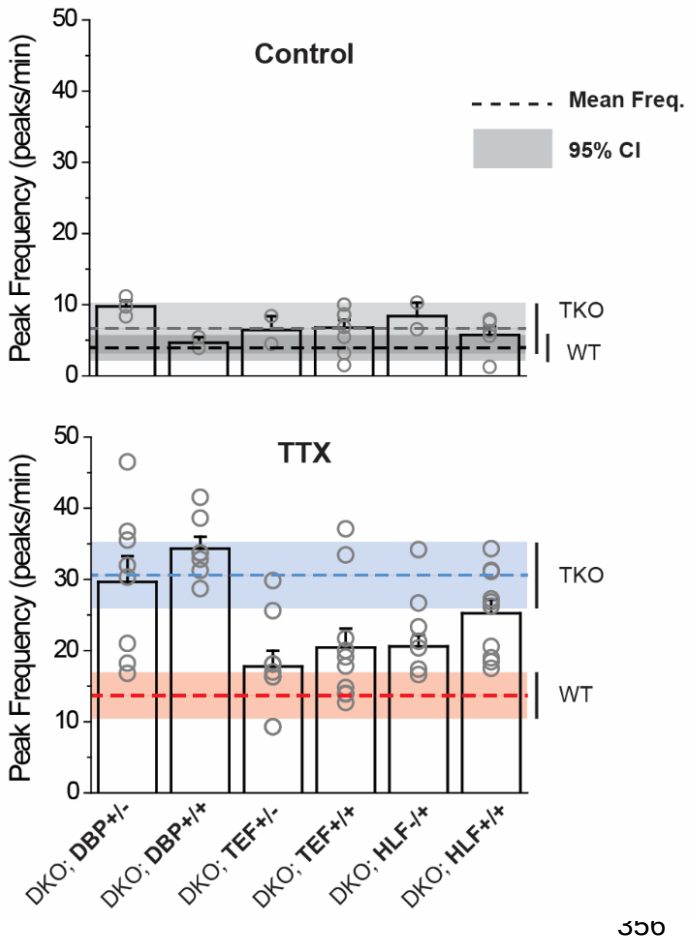

Figure 6. A single copy of *Hlf* or *Tef* is sufficient to maintain normal control of homeostatic plasticity in mutant mice. Quantification of network activity measured by the number of peaks/minute of GCamp6f fluorescence. Under control conditions (top panel), all genotypes had similar levels of activity (4.7-9.7 peaks/min) and WT and mutant 95% confidence intervals were overlapping. However, the effects of TTX (bottom panel) differed by genotype. Slices from animals with one or both copies of *Dbp* (first two columns) have activity that are not statistically different from those from TKO animals (blue dotted line) (adj.p = 0.99 and 0.99 respectively, two-way ANOVA with Tukey test for multiple comparisons). However slices from animals with either one or both copies of *Tef* (two middle columns) are significantly different from TTX-treated TKO (adj.p = 0.0015 for *Tef* heterozygous and adj.p = 0.027 for *Tef* WT) and were not significantly different from wild-type TTX-treated slices (adj. p = 0.98 and 0.526 respectively). A single copy of *Hlf* was not significantly different from WT (adj p = 0.79) but both copies were (adj. p = 0.0058). TTX slices with one or both copies of *Hlf* were not significantly different from TKO TTX-treated slices (adj. p = 0.18 and 0.85 respectively).

To further dissect the relative contribution of the Par bZIP family members we measured the survival of the mice with different numbers of copies of the TFs. TKO animals develop spontaneous seizures and have a dramatically decreased lifespan (Gachon et al., 2004). While our objective was not to make a detailed study of the seizure phenotype, we also observed, on multiple occasions, TKO animals that experienced spontaneous seizures, even though for most of cases, the instance of death was not directly observed. However, just one allele of either *Hlf* or *Tef* restores the lifespan of the animals to levels not statistically different from WT. Mice with one *Dbp* allele have improved survival compared to TKO animals but still die at a statistically significant higher rate than WT mice (Figure 7). These results differ from the cortical network activity response to activity deprivation in organotypic slices where the presence of *Dbp* had no effect on homeostatic plasticity constraint. These data suggest that even though *Dbp* is dispensable for restraining homeostatic plasticity in the cortex, it may play a role in preventing premature death by functioning elsewhere in the brain or peripheral tissue (Stewart et al., 2020) since these TF are expressed and play important roles there (Wahlestedt et al., 2017; Wang et al., 2010). However, a single allele of *Hlf* and *Tef* is enough to compensate for loss of the rest of the family members and restore survival to WT levels.

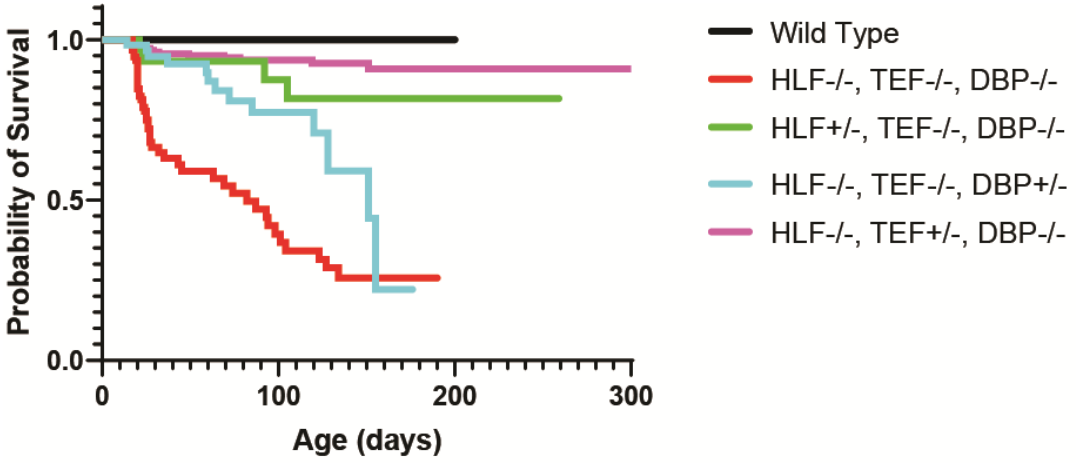

Figure 7. Presence of one allele of a PARbZIP TF improves survival relative to TKO animals. TKO mice have dramatically decreased survival (red line) compared to wild-type mice (black line). Presence of one copy of either *Hlf* (green line) or *Tef* (purple line) prevents premature death and the survival curves are not statistically different from wild-type, p = 0.118 and p = 0.562 respectively, Log-Rank test with Bonferroni correction for multiple comparisons. DBP heterozygous mice (blue line) also have improved survival over triple mutants (p = 0.003) but are still statistically more likely to die prematurely than wild-type mice (p = 0.0003).

Discussion

Inappropriately triggered homeostatic plasticity can either fail to compensate for changes in activity or can itself destabilize network activity (Nelson and Valakh, 2015). Although some molecular pathways that are required for the induction of homeostatic plasticity have been identified, whether and how homeostatic plasticity is negatively regulated is unknown. Here we show that reduced activity, which initiates a compensatory increase in network excitability, also activates a set of transcription factors that function to restrain homeostasis. Thus we propose a model in which homeostatic plasticity is negatively regulated through the PAR bZIP family of TFs.

Excitatory neurons respond to a global drop in network activity by upregulating the frequency and amplitude of excitatory synaptic currents, decreasing inhibitory currents and increasing intrinsic excitability. These changes correlate with dramatically increased network activity immediately following removal of activity blockade that “overshoots” initial activity levels. Synaptic scaling of excitatory synapses has previously been shown to depend on intact transcription and translation (Dörrbaum et al., 2020; Goold and Nicoll, 2010; Ibata et al., 2008; Schanzenbächer et al., 2016). Here we demonstrate a second role for transcription in regulating the strength of the network homeostatic response. Loss of *Hlf*, *Tef*, and *Dbp* results in exaggerated homeostatic changes. However, the levels of network activity at baseline are unchanged. This suggests that these transcription factors are activated to restrain homeostatic signaling rather than downregulating network dynamics directly. While a few other genes have been described that have limited effects on network dynamics, but are required for homeostatic plasticity (Shank3 (Tatavarty et al., 2020), FMRP (Soden and Chen, 2010), Caspr2 (Fernandes et al., 2019)), this is, to our knowledge, the first negative regulator of homeostasis to be described.

Present data implicates mEPSC frequency, but not amplitude, as the site of the restraint of homeostatic plasticity. We cannot eliminate the contribution of inhibitory neurons as the contributing factor to homeostatic plasticity restraint since *Hlf* and *Tef* are expressed in this neuronal type. Interneuron function may also be regulated by *Hlf* and *Tef* and this role may predispose the network to seizures. Dissecting the contribution of different cell types during different developmental windows will require generation of a conditional knock out and selective cell-type specific disruption of individual transcription factors at different times in development.

mIPSCs received by the excitatory neurons cannot explain the exaggerated network hyperexcitability caused by TTX incubation in TKO slices since neither the amplitude nor frequency of mIPSCs is different in the TTX condition. We note, however, that the amplitude of mIPSCs is decreased at baseline in the untreated cultures. Such decrease of the strength of inhibitory currents is insufficient on its own to induce network excitability but may make the network more vulnerable to future insults.

It is tempting to imagine a direct relationship between the exaggerated homeostatic plasticity in TKO cortical slices and the increased seizures and spontaneous death of mutant animals. The lack of constraint of homeostatic response can potentially explain, at least in part, the seizure phenotype in animals lacking all three TFs. However, partial genetic compensation of DBP for the survival phenotype but not the homeostatic plasticity phenotype as assayed by calcium imaging, suggests that the propensity to develop seizures and diminished survival have a more complex origin involving other brain regions and perhaps other organs of the body.

Gachon et al. (Gachon et al., 2004) first reported that deletion of the PARbZIP proteins TEF, HLF and DBP caused spontaneous and audiogenic seizures. They suggested that this may reflect effects on neurotransmitter metabolism caused by a reduction in pyridoxal phosphate (PLP) since pyridoxal kinase, which catalyzes the last step in the conversion of vitamin B6 into PLP is a target of the PAR bZIP proteins. PLP is a required cofactor for decarboxylases and other enzymes involved in the synthesis and metabolism of GABA, glutamate and the biogenic amine neurotransmitters including dopamine, serotonin and histamine. Using HPLC they found no changes in GABA or glutamate, but reduced levels of dopamine, serotonin and histamine in the knockout animals. Although changes in amine transmitters could potentially contribute to phenotypes in vivo, they are unlikely to contribute to plasticity in cortical slice cultures which do

not include the brainstem nuclei from which these projections arise. Reduced glutamate decarboxylase action could potentially have contributed to the observed baseline reduction in mIPSCs since heterozygous (Lazarus et al., 2015) and homozygous (Lau and Murthy, 2012) mutants of Gad1, the gene encoding the GAD67 isoform of glutamic acid decarboxylase, have reduced mIPSC amplitudes. However, this does not account for the enhanced homeostatic overshoot following activity blockade, since in the TKO animals, activity blockade did not produce any further reduction in inhibition, but produced robust changes at excitatory synapses.

HLF and TEF form homo- or heterodimers and recognize similar DNA sequences (Gachon, 2007). Here we demonstrate that these TFs can powerfully compensate for the loss of other family members. For instance, just one copy of *Tef* in the complete absence of *Hlf* and *Dbp* is sufficient to preserve the normal restraint of homeostatic plasticity, producing a response to activity deprivation that is indistinguishable from WT. Similarly, and in agreement with prior findings (Gachon et al., 2004), *Tef* and *Hlf* can robustly compensate for loss of each other and completely restore life span. Such robust compensation and functional redundancy of these TFs highlights their importance and may explain why they have not been identified in GWAS studies as risk factors for epilepsy or other neuropsychiatric diseases.

Besides their function in early embryonic development (Gavriouchkina et al., 2010; Wahlestedt et al., 2017), the PARb Zip TFs have been extensively studied for their roles in circadian rhythms in flies, zebrafish, and rodents (Cyran et al., 2003; Vatine et al., 2009; Weger et al., 2021). The present finding that HLF and TEF also act to restrain homeostatic plasticity is consistent with a recent report demonstrating that PAR bZIP TFs are differentially expressed in human epileptogenic tissue (Rambousek et al., 2020) In addition, CLOCK, an upstream regulator of these TFs, is necessary in cortical excitatory neurons for maintaining normal network activity and leads to epilepsy when conditionally deleted in these neurons (Li et al., 2017). Multiple components of the molecular clock are robustly expressed in the neocortex (Bering et al., 2018; Gachon et al., 2004; Kobayashi et al., 2015), consistent with the idea that they might have an additional function in the cortex that is distinct from their circadian role in SCN. However, the role of core clock genes in homeostatic plasticity has not yet been explored. In this work we expand the role of the PAR bZIP family of transcription factors to include the negative regulation of homeostatic plasticity.

Why should homeostatic plasticity be subject to such dual “push/pull” regulation? Perhaps because the changes in drive and excitability which must be buffered vary so widely during development. During the first few weeks of postnatal development in rodents, cortical neurons go from receiving few synapses to receiving thousands. This may require developmental downregulation of the strength of homeostatic plasticity. Neuropsychiatric diseases, such as monogenic causes of ASD, can trigger homeostatic changes in circuit properties which restore overall firing rates, but nonetheless have maladaptive effects on cortical function and flexibility (Antoine et al., 2019; Nelson and Valakh, 2015). Conversely, loss of function of genes giving rise to developmental disorders can cause failures of homeostatic plasticity (Blackman et al., 2012; Genç et al., 2020). Our findings provide a potential target for enhancing homeostatic plasticity in contexts where it is insufficient or for downregulating it when it is maladaptive, and provide an avenue to identify how the positive and negative regulators of homeostasis interact to stabilize network activity.

Material and Methods

Animals

All procedures were approved by the Institutional Animal Care and Use Committee at Brandeis University, and conformed to the National Institutes of Health Guide for the Care and Use of Laboratory Animals. The initial RNAseq screen (Figure 1) was performed using the cre-dependent tdTomato reporter strain Ai9 (Madisen et al., 2010) crossed with either parvalbumin-ires-cre (Hippenmeyer et al., 2005) , or Emx1-ires-cre animals (Gorski et al., 2002) obtained from Jackson Labs. All other experiments were performed using wild-type (WT; C57BL/6J) and previously published HLF, TEF, DBP triple mutant animals (Gachon et al., 2004) which were acquired from the European Mouse Mutant Archive (stock EM:02489) as frozen embryos and propagated via IVF using a provider-recommended protocol. *Hlf*, *Tef*, *Dbp* mutant mice were housed on a 12/12 light/dark cycle in a dedicated, climate-controlled facility. Cages were enriched with huts, chew sticks, and tubes. Food and water were available *ad libitum*, and animals were housed in groups of 2-4 after weaning at p21. Mice of both sexes were used for experiments.

Organotypic Slice Culture

Organotypic slices were dissected from P6-8 pups. Animals were anaesthetized with a ketamine (20 mg/mL), xylazine (2.5 mg/mL) and acepromazine (0.5 mg/mL) mixture (40 µL, via intraperitoneal injection), the brain was extracted, embedded in 2% agarose, and coronal slices containing primary somatosensory cortex were cut on a compresstome (Precisionary Instruments, Greenville, NC) to 300 µm in ice-chilled ACSF (126 mM NaCl, 25 mM NaHCO3, 3 mM KCl, 1 mM NaH_2PO_4, 25 mM dextrose, 2 mM $CaCl_2$ and 2 mM $MgCl_2$, 315-319 mOsm) with a ceramic blade and placed directly onto 6-well Millipore Millicell cell culture inserts (Millipore Sigma PICM0RG50, Burlington, Massachusetts) over 1 mL warmed neuronal media (1x MEM (Millipore-Sigma), 1x GLUTAMAX (Gibco Thermo-Fisher Scientific), 1 mM $CaCl_2$, 2 mM $MgSO_4$, 12.9 mM dextrose, 0.08% ascorbic acid, 18 mM $NaHCO_3$, 35 mM 1M HEPES (pH 7.5), 1 µg/mL insulin and 20% Horse Serum (heat inactivated, Millipore-Sigma, Burlington, Massachusetts), pH 7.45 and 305 mOsm). Slices were placed in media containing 1x PenStrep (Gibco Thermo-Fisher Scientific) and 50 µg/mL gentamicin (Millipore-Sigma for 24 hours and subsequent media changes were antibiotic-free. The slices were then grown at 35^{o}C and 5% CO_2. Media was changed every other day to 1 mL fresh media. For TTX treatment, media containing 500nM TTX was added during the media change at EP 12. For TTX washout experiments, two additional media changes with TTX-free media were performed 5 minutes apart.

RNA-sequencing

Cell sorting: Slice cultures were converted into a single cell suspension as previously described (Sugino et al., 2006), with some modifications. Organotypic slice cultures were placed in ice cold, oxygenated ACSF with 1% FBS and 5% Trehalose (Saxena et al., 2012), that had been 0.4 µm filtered, containing blockers (APV, DNQX and TTX) to prevent excitotoxicity, and gently removed from the membrane. The cortex was micro-dissected under a Leica MZ 16-F fluorescent microscope and the tissue placed in an oxygenated room temperature bath for 45 minutes, supplemented with 1 mg/ml type XIV protease (Sigma-Aldrich). Afterwards the tissue

was moved back to the ACSF solution (without protease) and triturated with fire polished Pasteur pipettes of successfully smaller diameters (~600, 300 and 150 μm). Samples were then sorted with a BD FACSAria Flow Cytometer. All isolated material for mRNA sequencing was harvested using the picopure RNA isolation kit (Life Technologies) and subjected to an on column DNAase digestion. mRNA libraries were prepared as previously described (O'Toole et al., 2017): amplifying with the Ovation RNA-seq system (Nugen), sonicating with a Covaris S 220 Shearing Device, constructing the libraries with the Ovation Rapid DR multiplex System (Nugen), and quantifying library concentration using the Illumina library quantification kit (KAPA biosystems). Samples were sequenced on either the Illumina Nextseq or Hiseq machines to a depth of ~25 million reads. Illumina sequencing adapters were trimmed from reads using cutadapt followed by mapping to the mm10 genome with STAR using the ENCODE Long RNA-Seq pipeline's parameters. Reads mapping to exons of known genes were quantified using featureCounts in the *Rsubread* pacakge (Liao et al., 2019) and differential expression analysis was conducted using DESeq2 (Love et al., 2014). Adjusted p-values for each gene are reported from a Wald Test evaluating the significance of the coefficient representing the treatment group (TTX or Control) followed by the Benjamini-Hochberg correction.

Quantitative real-time PCR.

RNA was extracted from neocortical regions of slice cultures using Trizol reagent followed by RNA Clean & Concentrator kit (Zymo research R1014). cDNA was synthesized with 0.5μg of RNA using the cDNA Synthesis Kit (Bio-Rad 170-8891) using random hexamers to generate cDNA from total RNA. Quantitative real-time PCR was performed using Corbett Research RG-6000 Real Time PCR Thermocycler with SYBR Green Supermix (Bio-Rad). The following primer sequences were used: RPL10 (forward) 5'-CACGGCAGAAACGAGACTTT-3', RPL10 (reverse) 5'-CACGGACGATCCTATTGTCA-3', GAPDH (forward) 5'-TCAATGAAGGGGTCGTTGAT-3' GAPDH (reverse) 5'-CGTCCCGTAGACAAAATGGT-3', HLF (forward) 5'-CGGTCATGGATCTCAGCAG-3', HLF (reverse) 5'-GTACCTGGATGGTGTCAGGG-3', TEF (forward) 5'-GAGCATTCTTTGCCTTGGTC-3', TEF (reverse) 5'-GGATGGTCTTGTCCCAGATG -3'.

Electrophysiology

Organotypic slice cultures were cut out of the cell culture inserts along with the membrane using a scalpel blade. Slices were transferred to a thermo-regulated recording chamber and continuously perfused with oxygenated ACSF. Neurons were visualized on an Olympus upright epifluorescence microscope with 10x air and 40x water immersion objectives. Visually guided whole cell patch-clamp recordings were made using near-infrared differential interference contrast microscopy. Recording pipettes of 3–5 MΩ resistance contained internal solution with the following concentrations. For excitatory currents and intrinsic excitability: (in mM) 20 KCl, 100 K-gluconate, 10 HEPES, 4 Mg-ATP, 0.3 Na-GTP, 10 Na-phosphocreatine, and 0.1% biocytin. For inhibitory currents: (in mM) 120 KCl, 10 HEPES, 4 Mg-ATP, 0.3 Na-GTP, 10 Na-phosphocreatine, and 0.1% biocytin. Recordings were collected using an AxoPatch 200B amplifier (Axon Instruments, Foster City, CA), filtered at 10 kHz and were not corrected for liquid

junction potentials. Data were collected on a Dell computer using custom software running on Igor Pro (WaveMetrics, Lake Oswego, OR).

Intrinsic excitability

Cells were selected at random from Layer 5 in primary somatosensory area of the cortex. Whole cell recordings were performed with a K-Gluconate-based internal recording solution. Synaptic currents were blocked by adding picrotoxin (PTX) at 25 µM, 6,7-dinitroquinoxaline-2,3-dione (DNQX) 25 µM, and (2R)-amino-5-phosphonovaleric acid (APV) at 35 µM to standard ACSF to block γ-aminobutyric acid (GABA), α-amino-3-hydroxy-5-methyl-4-isoxazolepropionic acid (AMPA), and N-methyl-d-aspartate (NMDA) receptors, respectively. Cells were held at -65mV by injecting a small current. 500 ms current injections ranging from -25 to 275 pA in 25pA steps increments at random intensity were delivered every 10 seconds. Adaptation ratio was calculated using custom-written IGOR script as previously described (Hattox and Nelson, 2007). Briefly, we calculated the ratio between the third and last inter-spike interval at two times the threshold current.

Synaptic currents

To isolated miniature excitatory AMPA-mediated currents 25µM PTX, 35µM APV and 500nM TTX were added to the extracellular recording solution. To isolate inhibitory currents, 20µM DNQX, 35µM APV and 500nM TTX were added to the extracellular solution. Cells were clamped at -65mV with a series resistance of below 20MΩ with no compensation for the liquid junction potential. 10 10-second traces were acquired for each cell. Miniature PSCs and action potentials were analyzed using custom-written IGOR scripts.

Calcium imaging

To visualized calcium dynamics, 24 hours after slice preparation, 1µL of pAAV.Syn.GCaMP6f.WPRE.SV40 (AAV9 capsid serotype, Addgene 100837) was applied to the somatosensory cortex in each hemisphere. At day EP14 slices were cut out along with the membrane and placed into the perfusion chamber mounted on a spinning disc microscope (Leica DMI 6000B (Leica Microsystems, Inc., Buffalo Grove, IL), with an Andor CSU W1 spinning disc unit, using an Andor Neo sCMOS cameras and Andor IQ3 to run the system (Andor Technology PLC, Belfast, N. Ireland). Slices were allowed to acclimate while being perfused with 33^{o}C oxygenated ACSF with no TTX for 10 minutes. Slices were imaged with a 10x objective centered over the primary somatosensory area. For each slice ten minutes of imaging from a 500µm square per slice were acquired at 33 frames per second.

Calcium Imaging analysis

Cellular somatic ROIs were selected by hand from background using custom MATLAB code (http://github.com/VH-Lab/vhlab-TwoPhoton-matlab) based on a standard deviation projection of the video (Figure 1A, bottom panel). Cells were only considered as viable if they: were of a characteristic size and shape for neurons; were bright enough to be clearly distinguished from background; were in focus with clear and sharp edges; and had several bouts of firing within the first minute. Only experiments where at least 15 such cells were analyzed were considered in further analysis. From these ROIs, mean intensity per cell at each frame was computed. The raw intensity value was transformed to ΔF/F by finding baseline values where the coefficient of variation within 50 frames was below 0.3 ΔF/F units/frame. In cases where we failed to find any

607 periods where the coefficient of variation was low, the 5th percentile of all values defined the
608 baseline. To produce a cellular firing frequency, noise was reduced by fitting the ΔF/F data with
609 a smoothing spline, then periods with a slope above 0.30 ΔF/F units/frame that were within 30
610 frames of other frames with positive slope were recorded. The number of such periods reflected
611 the number of times each cell was active during a minute, though this measure had no ability to
612 predict the number of action potentials that made up each firing period.

613

614

615 **References**

616 Antoine, M.W., Langberg, T., Schnepel, P., and Feldman, D.E. (2019). Increased Excitation-
617 Inhibition Ratio Stabilizes Synapse and Circuit Excitability in Four Autism Mouse Models.
618 Neuron *101*, 648-661.e4.

619 Bering, T., Carstensen, M.B., Wörtwein, G., Weikop, P., and Rath, M.F. (2018). The Circadian
620 Oscillator of the Cerebral Cortex: Molecular, Biochemical and Behavioral Effects of Deleting the
621 Arntl Clock Gene in Cortical Neurons. Cereb. Cortex *28*, 644–657.

622 Blackman, M.P., Djukic, B., Nelson, S.B., and Turrigiano, G.G. (2012). A critical and cell-
623 autonomous role for MeCP2 in synaptic scaling up. J. Neurosci. Off. J. Soc. Neurosci. *32*,
624 13529–13536.

625 Cyran, S.A., Buchsbaum, A.M., Reddy, K.L., Lin, M.-C., Glossop, N.R.J., Hardin, P.E., Young,
626 M.W., Storti, R.V., and Blau, J. (2003). vrille, Pdp1, and dClock form a second feedback loop in
627 the Drosophila circadian clock. Cell *112*, 329–341.

628 Davis, G.W. (2006). Homeostatic control of neural activity: from phenomenology to molecular
629 design. Annu. Rev. Neurosci. *29*, 307–323.

630 Delvendahl, I., and Müller, M. (2019). Homeostatic plasticity-a presynaptic perspective. Curr.
631 Opin. Neurobiol. *54*, 155–162.

632 Desai, N.S., Rutherford, L.C., and Turrigiano, G.G. (1999). Plasticity in the intrinsic excitability of
633 cortical pyramidal neurons. Nat. Neurosci. *2*, 515–520.

634 Desai, N.S., Cudmore, R.H., Nelson, S.B., and Turrigiano, G.G. (2002). Critical periods for
635 experience-dependent synaptic scaling in visual cortex. Nat. Neurosci. *5*, 783–789.

636 Dörrbaum, A.R., Alvarez-Castelao, B., Nassim-Assir, B., Langer, J.D., and Schuman, E.M.
637 (2020). Proteome dynamics during homeostatic scaling in cultured neurons. ELife *9*, e52939.

638 Fernandes, D., Santos, S.D., Coutinho, E., Whitt, J.L., Beltrão, N., Rondão, T., Leite, M.I.,
639 Buckley, C., Lee, H.-K., and Carvalho, A.L. (2019). Disrupted AMPA Receptor Function upon
640 Genetic- or Antibody-Mediated Loss of Autism-Associated CASPR2. Cereb. Cortex N. Y. NY *29*,
641 4919–4931.

642 Gachon, F. (2007). Physiological function of PARbZip circadian clock-controlled transcription
643 factors. Ann. Med. *39*, 562–571.

644 Gachon, F., Fonjallaz, P., Damiola, F., Gos, P., Kodama, T., Zakany, J., Duboule, D., Petit, B.,
645 Tafti, M., and Schibler, U. (2004). The loss of circadian PAR bZip transcription factors results in
646 epilepsy. Genes Dev. *18*, 1397–1412.

647 Galvan, C.D., Hrachovy, R.A., Smith, K.L., and Swann, J.W. (2000). Blockade of Neuronal
648 Activity During Hippocampal Development Produces a Chronic Focal Epilepsy in the Rat. J.
649 Neurosci. *20*, 2904–2916.

650 Gavriouchkina, D., Fischer, S., Ivacevic, T., Stolte, J., Benes, V., and Dekens, M.P.S. (2010).
651 Thyrotroph embryonic factor regulates light-induced transcription of repair genes in zebrafish
652 embryonic cells. PloS One *5*, e12542.

653 Genç, Ö., An, J.-Y., Fetter, R.D., Kulik, Y., Zunino, G., Sanders, S.J., and Davis, G.W. (2020).
654 Homeostatic plasticity fails at the intersection of autism-gene mutations and a novel class of
655 common genetic modifiers. ELife *9*, e55775.

656 Goold, C.P., and Nicoll, R.A. (2010). Single-cell optogenetic excitation drives homeostatic
657 synaptic depression. Neuron *68*, 512–528.

658 Gorski, J.A., Talley, T., Qiu, M., Puelles, L., Rubenstein, J.L.R., and Jones, K.R. (2002). Cortical
659 Excitatory Neurons and Glia, But Not GABAergic Neurons, Are Produced in the Emx1-
660 Expressing Lineage. J. Neurosci. *22*, 6309–6314.

661 Hattox, A.M., and Nelson, S.B. (2007). Layer V Neurons in Mouse Cortex Projecting to Different
662 Targets Have Distinct Physiological Properties. J. Neurophysiol. *98*, 3330–3340.

663 Hawkins, N.A., and Kearney, J.A. (2012). Confirmation of an epilepsy modifier locus on mouse
664 chromosome 11 and candidate gene analysis by RNA-Seq. Genes Brain Behav. *11*, 452–460.

665 Hawkins, N.A., and Kearney, J.A. (2016). Hlf is a genetic modifier of epilepsy caused by
666 voltage-gated sodium channel mutations. Epilepsy Res. *119*, 20–23.

667 Hippenmeyer, S., Vrieseling, E., Sigrist, M., Portmann, T., Laengle, C., Ladle, D.R., and Arber,
668 S. (2005). A Developmental Switch in the Response of DRG Neurons to ETS Transcription
669 Factor Signaling. PLoS Biol. *3*, e159.

670 Hobbiss, A.F., Ramiro-Cortés, Y., and Israely, I. (2018). Homeostatic Plasticity Scales Dendritic
671 Spine Volumes and Changes the Threshold and Specificity of Hebbian Plasticity. IScience *8*,
672 161–174.

673 Ibata, K., Sun, Q., and Turrigiano, G.G. (2008). Rapid Synaptic Scaling Induced by Changes in
674 Postsynaptic Firing. Neuron *57*, 819–826.

675 Johnson, H.A., and Buonomano, D.V. (2007). Development and Plasticity of Spontaneous
676 Activity and Up States in Cortical Organotypic Slices. J. Neurosci. *27*, 5915–5925.

677 Karmarkar, U.R., and Buonomano, D.V. (2006). Different forms of homeostatic plasticity are
678 engaged with distinct temporal profiles. Eur. J. Neurosci. *23*, 1575–1584.

679 Kilman, V., Rossum, M.C.W. van, and Turrigiano, G.G. (2002). Activity Deprivation Reduces
680 Miniature IPSC Amplitude by Decreasing the Number of Postsynaptic GABAA Receptors
681 Clustered at Neocortical Synapses. J. Neurosci. *22*, 1328–1337.

682 Kim, J., and Alger, B.E. (2010). Reduction in endocannabinoid tone is a homeostatic
683 mechanism for specific inhibitory synapses. Nat. Neurosci. *13*, 592–600.

684 Kobayashi, Y., Ye, Z., and Hensch, T.K. (2015). Clock genes control cortical critical period
685 timing. Neuron *86*, 264–275.

686 Koch, H., Huh, S.-E., Elsen, F.P., Carroll, M.S., Hodge, R.D., Bedogni, F., Turner, M.S., Hevner,
687 R.F., and Ramirez, J.-M. (2010). Prostaglandin E2-Induced Synaptic Plasticity in Neocortical
688 Networks of Organotypic Slice Cultures. J. Neurosci. *30*, 11678–11687.

689 Lambo, M.E., and Turrigiano, G.G. (2013). Synaptic and Intrinsic Homeostatic Mechanisms
690 Cooperate to Increase L2/3 Pyramidal Neuron Excitability during a Late Phase of Critical Period
691 Plasticity. J. Neurosci. *33*, 8810–8819.

692 Lau, C.G., and Murthy, V.N. (2012). Activity-Dependent Regulation of Inhibition via GAD67. J.
693 Neurosci. *32*, 8521–8531.

694 Lazarus, M.S., Krishnan, K., and Huang, Z.J. (2015). GAD67 deficiency in parvalbumin
695 interneurons produces deficits in inhibitory transmission and network disinhibition in mouse
696 prefrontal cortex. Cereb. Cortex N. Y. N 1991 *25*, 1290–1296.

697 Li, P., Fu, X., Smith, N.A., Ziobro, J., Curiel, J., Tenga, M.J., Martin, B., Freedman, S., Cea-Del
698 Rio, C.A., Oboti, L., et al. (2017). Loss of CLOCK Results in Dysfunction of Brain Circuits
699 Underlying Focal Epilepsy. Neuron *96*, 387-401.e6.

700 Liao, Y., Smyth, G.K., and Shi, W. (2019). The R package Rsubread is easier, faster, cheaper
701 and better for alignment and quantification of RNA sequencing reads. Nucleic Acids Res. *47*,
702 e47.

703 Love, M.I., Huber, W., and Anders, S. (2014). Moderated estimation of fold change and
704 dispersion for RNA-seq data with DESeq2. Genome Biol. *15*, 550.

705 Madisen, L., Zwingman, T.A., Sunkin, S.M., Oh, S.W., Zariwala, H.A., Gu, H., Ng, L.L., Palmiter,
706 R.D., Hawrylycz, M.J., Jones, A.R., et al. (2010). A robust and high-throughput Cre reporting
707 and characterization system for the whole mouse brain. Nat. Neurosci. *13*, 133–140.

708 Mitsui, S., Yamaguchi, S., Matsuo, T., Ishida, Y., and Okamura, H. (2001). Antagonistic role of
709 E4BP4 and PAR proteins in the circadian oscillatory mechanism. Genes Dev. *15*, 995–1006.

710 Moore, A.R., Richards, S.E., Kenny, K., Royer, L., Chan, U., Flavahan, K., Van Hooser, S.D.,
711 and Paradis, S. (2018). Rem2 stabilizes intrinsic excitability and spontaneous firing in visual
712 circuits. ELife *7*, e33092.

713 Nelson, S.B., and Valakh, V. (2015). Excitatory/Inhibitory Balance and Circuit Homeostasis in
714 Autism Spectrum Disorders. Neuron *87*, 684–698.

715 O'Toole, S.M., Ferrer, M.M., Mekonnen, J., Zhang, H., Shima, Y., Ladle, D.R., and Nelson, S.B.
716 (2017). Dicer maintains the identity and function of proprioceptive sensory neurons. J.
717 Neurophysiol. *117*, 1057–1069.

718 Rambousek, L., Gschwind, T., Lafourcade, C., Paterna, J.-C., Dib, L., Fritschy, J.-M., and
719 Fontana, A. (2020). Aberrant expression of PAR bZIP transcription factors is associated with
720 epileptogenesis, focus on hepatic leukemia factor. Sci. Rep. *10*, 1–16.

721 Ripperger, J.A., Shearman, L.P., Reppert, S.M., and Schibler, U. (2000). CLOCK, an essential
722 pacemaker component, controls expression of the circadian transcription factor DBP. Genes
723 Dev. *14*, 679–689.

724 Sanchez-Vives, M.V., and McCormick, D.A. (2000). Cellular and network mechanisms of
725 rhythmic recurrent activity in neocortex. Nat. Neurosci. *3*, 1027–1034.

726 Saxena, A., Wagatsuma, A., Noro, Y., Kuji, T., Asaka-Oba, A., Watahiki, A., Gurnot, C.,
727 Fagiolini, M., Hensch, T.K., and Carninci, P. (2012). Trehalose-enhanced isolation of neuronal
728 sub-types from adult mouse brain. BioTechniques *52*, 381–385.

729 Schanzenbächer, C.T., Sambandan, S., Langer, J.D., and Schuman, E.M. (2016). Nascent
730 Proteome Remodeling following Homeostatic Scaling at Hippocampal Synapses. Neuron *92*,
731 358–371.

732 Scharfman, H. (2002). A Novel Animal Model of Epilepsy Caused by Inhibiting Neuronal Activity
733 during Development. Epilepsy Curr. *2*, 127–128.

734 Schaukowitch, K., Reese, A.L., Kim, S.-K., Kilaru, G., Joo, J.-Y., Kavalali, E.T., and Kim, T.-K.
735 (2017). An Intrinsic Transcriptional Program Underlying Synaptic Scaling during Activity
736 Suppression. Cell Rep. *18*, 1512–1526.

737 Soden, M.E., and Chen, L. (2010). Fragile X Protein FMRP Is Required for Homeostatic
738 Plasticity and Regulation of Synaptic Strength by Retinoic Acid. J. Neurosci. *30*, 16910–16921.

739 Stellwagen, D., and Malenka, R.C. (2006). Synaptic scaling mediated by glial TNF-α. Nature
740 *440*, 1054.

741 Stewart, M., Silverman, J.B., Sundaram, K., and Kollmar, R. (2020). Causes and Effects
742 Contributing to Sudden Death in Epilepsy and the Rationale for Prevention and Intervention.
743 Front. Neurol. *11*, 765.

744 Sugino, K., Hempel, C.M., Miller, M.N., Hattox, A.M., Shapiro, P., Wu, C., Huang, Z.J., and
745 Nelson, S.B. (2006). Molecular taxonomy of major neuronal classes in the adult mouse
746 forebrain. Nat. Neurosci. *9*, 99–107.

747 Sun, Q., and Turrigiano, G.G. (2011). PSD-95 and PSD-93 Play Critical But Distinct Roles in
748 Synaptic Scaling Up and Down. J. Neurosci. *31*, 6800–6808.

749 Tan, H.L., Queenan, B.N., and Huganir, R.L. (2015). GRIP1 is required for homeostatic
750 regulation of AMPAR trafficking. Proc. Natl. Acad. Sci. *112*, 10026–10031.

751 Tatavarty, V., Pacheco, A.T., Kuhnle, C.G., Lin, H., Koundinya, P., Miska, N.J., Hengen, K.B.,
752 Wagner, F.F., Hooser, S.D.V., and Turrigiano, G.G. (2020). Autism-associated Shank3 is
753 essential for homeostatic compensation in rodent V1. Neuron *106*, 769-777.e4.

754 Turrigiano, G.G., and Nelson, S.B. (2004). Homeostatic plasticity in the developing nervous
755 system. Nat. Rev. Neurosci. *5*, 97.

756 Turrigiano, G.G., Leslie, K.R., Desai, N.S., Rutherford, L.C., and Nelson, S.B. (1998). Activity-
757 dependent scaling of quantal amplitude in neocortical neurons. Nature *391*, 892–896.

758 Vatine, G., Vallone, D., Appelbaum, L., Mracek, P., Ben-Moshe, Z., Lahiri, K., Gothilf, Y., and
759 Foulkes, N.S. (2009). Light Directs Zebrafish period2 Expression via Conserved D and E Boxes.
760 PLoS Biol. *7*, e1000223.

761 Wahlestedt, M., Ladopoulos, V., Hidalgo, I., Sanchez Castillo, M., Hannah, R., Säwén, P., Wan,
762 H., Dudenhöffer-Pfeifer, M., Magnusson, M., Norddahl, G.L., et al. (2017). Critical Modulation of
763 Hematopoietic Lineage Fate by Hepatic Leukemia Factor. Cell Rep. *21*, 2251–2263.

764 Wallace, W., and Bear, M.F. (2004). A Morphological Correlate of Synaptic Scaling in Visual
765 Cortex. J. Neurosci. *24*, 6928–6938.

766 Wang, Q., Maillard, M., Schibler, U., Burnier, M., and Gachon, F. (2010). Cardiac hypertrophy,
767 low blood pressure, and low aldosterone levels in mice devoid of the three circadian PAR bZip
768 transcription factors DBP, HLF, and TEF. Am. J. Physiol.-Regul. Integr. Comp. Physiol. *299*,
769 R1013–R1019.

770 Wang, Q., Chiu, S.-L., Koropouli, E., Hong, I., Mitchell, S., Easwaran, T.P., Hamilton, N.R.,
771 Gustina, A.S., Zhu, Q., Ginty, D.D., et al. (2017). Neuropilin-2/PlexinA3 Receptors Associate
772 with GluA1 and Mediate Sema3F-Dependent Homeostatic Scaling in Cortical Neurons. Neuron
773 *96*, 1084-1098.e7.

774 Weger, B.D., Gobet, C., David, F.P.A., Atger, F., Martin, E., Phillips, N.E., Charpagne, A.,
775 Weger, M., Naef, F., and Gachon, F. (2021). Systematic analysis of differential rhythmic liver
776 gene expression mediated by the circadian clock and feeding rhythms. Proc. Natl. Acad. Sci. U.
777 S. A. *118*, e2015803118.

778 Wierenga, C.J., Walsh, M.F., and Turrigiano, G.G. (2006). Temporal Regulation of the
779 Expression Locus of Homeostatic Plasticity. J. Neurophysiol. *96*, 2127–2133.

780 Yoshimura, T., and Rasband, M.N. (2014). Axon initial segments: diverse and dynamic neuronal
781 compartments. Curr. Opin. Neurobiol. *27*, 96–102.

782